MNRAS 000, 1–7 (2023) Preprint 7 September 2023 Compiled using MNRAS LATEX style file v3.0

Modeling the Stellar Evolution of Hypervelocity Runaways from Thermonuclear Supernovae

Aakash Bhat,[1,2]★ Evan B. Bauer,[3] Ilaria Caiazzo,[4] Rüdiger Pakmor,[5] Abinaya Swaruba Rajamuthukumar,[5] Ken J. Shen,[6] Kareem El-Badry,[4] Jim Fuller,[4] Wolfgang E. Kerzendorf,[7] Stephen Justham[5]

[1]*Institut für Physik und Astronomie, Universität Potsdam, Haus 28, Karl-Liebknecht-Str. 24/25, 14476 Potsdam-Golm, Germany*
[2]*Dr Karl Remeis-Observatory & ECAP, Friedrich-Alexander University Erlangen-Nürnberg, Sternwartstr. 7, 96049 Bamberg, Germany*
[3]*Center for Astrophysics | Harvard & Smithsonian, 60 Garden Street, Cambridge, MA 02138, USA*
[4]*Division of Physics, Mathematics and Astronomy, California Institute of Technology, 1200 E. California Blvd., Pasadena, CA 91125, USA*
[5]*Max Planck Institut für Astrophysik, Karl-Schwarzschild-Straße 1, 85748 Garching bei München, Germany*
[6] *Department of Astronomy and Theoretical Astrophysics Center, University of California, Berkeley, CA 94720-3411, USA*
[7] *Department of Physics and Astronomy, Michigan State University, East Lansing, MI 48824, USA*

Accepted XXX. Received YYY; in original form ZZZ

ABSTRACT

The fastest runaway stars in our Galaxy are produced by supernovae in very compact double white dwarf binaries. Their measured velocities alone provide strong constraints on the configurations of the binaries that produced them at the moment of supernova explosion. We have observed the runaway stellar remnants a hundred thousand to a few million years after they were released from their companion supernova at $\approx 2000 \mathrm{kms}^{-1}$, but their current stellar structure is very different from the compact configuration they must have had in a double white dwarf binary. No detailed stellar evolution simulations have yet succeeded in reproducing and explaining their currently inflated and luminous states, and recent discoveries have provided fresh motivation for stellar evolution models to compare to the growing population of these hypervelocity runaways. Existing simulations of the hydrodynamics in the binary leading up to supernova detonation provide an excellent starting point for building models to explore the subsequent stellar evolution of the runaway donor using MESA. In this report we describe our work on the first such evolutionary models. We show here that such modeling might explain at least some of the remnants, if not all. As future outlook we also provide a prescription for further using these methods for modeling Type-Iax supernova remnants as well as other compact objects like subdwarfs which might be remnants of thermonuclear supernovas as well.

Key words: Hyper-velocity stars – Type-Ia – White Dwarf

1 INTRODUCTION

Hypervelocity stars are stars with velocities greater than the escape velocity of the Galaxy. Such objects have different progenitor systems, including Supernovae of Type Ia. In this scenario a compact star, either a stripped He star or a WD, transfers mass to a WD. This mass transfer, mainly due to the ^{4}He can trigger an explosion in the white dwarf, known as a thermonuclear supernova. Once this happens the donor star is flung out at the orbital speed of the binary, which due to the compact nature of the stars can reach speeds of the order $> 1000 \mathrm{\ km\ s}^{-1}$.

Recent observations have observed the fastest such stars in the galaxy coming from the D6 (dynamically driven double degenerate double detonation) channel (Shen et al. 2018; El-Badry et al. 2023) as well as hypervelocity stars from partial detonations in Type Iax supernovae (Raddi et al. 2019) and from mass transfer through a He-subdwarf (Hirsch et al. 2005; Geier et al. 2015). Out of all these, the D6 stars are the most peculiar, as despite being white dwarfs some of them lie at the end of the horizontal branch in the color-magnitude diagram, where one would expect subdwarfs and where US-708 indeed lies. One of the reasons that has been theorized for this behaviour is due to the ejected material deposited by the supernova explosion of the primary, wherein attempts have previously been made to understand this phenomenon by Bauer et al. (2019) for subdwarfs and by Zhang et al. (2019) for type Iax remnants.

While these efforts have provided key insights into the evolution of such stars, a more detailed investigation into the evolution of such stars, in particular due to their peculiar chemical composition, is still missing. This is particularly interesting as Type-Ia supernovae produce radioactive Nickel which can alter the composition and evolution of the donor white dwarf drastically (Kuchner et al. 1994) after it is deposited by the supernova ejecta. In this project we utilize the results of Arepo 3-dimensional hydro-dynamical simulations of binary white dwarfs which undergo supernova explosions (Pakmor et al. 2022) as inputs for the open-source stellar evolution software MESA (Paxton et al. 2011, 2013, 2015, 2018, 2019; Jermyn et al. 2023). This allowed us to relax and evolve a white dwarf which has been contaminated by supernova ejecta from another white dwarf to find its evolutionary track, by inputting relevant parameters like

★ E-mail: aakashbhat7@gmail.com

the temperature-density profile and the new composition from the Arepo simulations. This project was subdivided into smaller modules, and this report is structured according to them. The modules can be categorized as: simulating the binary system and getting relevant parameters, relaxing white dwarf models in MESA using these parameters, evolving the relaxed star to observable lifetimes and comparison with observations, and finally a prescription for continuing this work for other models.

2 SIMULATIONS AND RELAXATION

The composition and entropy files are taken from the work of Pakmor et al. (2022), using the 3 dimensional hydrodynamics code Arepo (Weinberger et al. 2020). In this particular simulation a white dwarf of $0.7 M_\odot$ is considered as the donor while the primary has a mass of $1.05 M_\odot$. As the primary is more massive and therefore smaller, the lighter white dwarf fills its Roche lobe first when sufficiently near to the primary. The primary then starts accreting mass, a significant fraction of which is Helium. This Helium is accumulated at the surface of the primary and dynamics in the dense accretion stream lead to violent burning. This first detonation at the surface ignites the interior of the primary which is composed of Carbon and Oxygen. This process results in a Type-Ia supernova, in the aftermath of which only the donor remains. However, before the donor can escape, the supernova ejecta traveling at $5000 - 15000\ \mathrm{kms}^{-1}$ (Pakmor et al. 2022) hits it. During this process, the secondary first loses a certain amount of its shell, while new material (in particular ^{56}Ni) is deposited from the ejecta resulting in a final mass of $0.67 M_\odot$. Furthermore, the supernova shock significantly heats up the white dwarf by depositing entropy behind the shock wave that traverses the WD interior.

The final Arepo composition profile contains 55 isotopes and temperature-density pairs for different zones of the star. Since MESA is a 1D evolutionary code, these 3D profiles are averaged over spherical shells. These profiles along with the mass coordinates relate to a specific case of a Type-Ia remnant which is not directly available in MESA. Therefore, we use the relaxation routines of MESA which are coordinate transformations of the temperature, density, and composition in the basis that MESA evolves in as shown in equation 1

$$\{\vec{T_i}, \vec{\rho_i}, \vec{\mathbf{X}_i}\} \longrightarrow \{\vec{T_f}, \vec{\rho_f}, \vec{\mathbf{X}_f}\} \tag{1}$$

To get a final WD model which can be relaxed to our compositions and entropy, we use the `make_co_wd` and `make_WD_model` routines within the test suite of MESA. We allow this model to relax to a final mass of 0.64 $M_\odot$. We use 0.64 as an approximation of the mass lost due to a surface cut, which we do at the mass coordinate where the energy due to Ni-56 decay is twice the binding energy due to gravity as shown in Fig. 1. Gravitational binding energy (per unit mass) is defined as Gm/r, while we estimated Ni decay energy as $(5.38\,\mathrm{MeV}) X_{\mathrm{Ni}}/(56 m_{\mathrm{p}})$ from the total energy of the decay chain $^{56}\mathrm{Ni} \rightarrow ^{56}\mathrm{Co} \rightarrow ^{56}\mathrm{Fe}$.

The final relaxation profile and composition of the main elements used is shown as a comparison in Fig. 2 and Fig. 3.

3 EVOLUTION

3.1 Factors affecting the evolution

Once we had the relaxed white dwarf model, the next step was creating evolutionary tracks. Due to the complexity of the composition

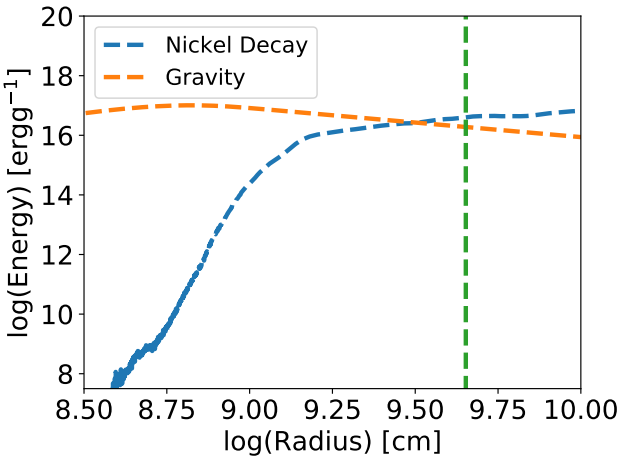

Figure 1. Comparison of Ni-56 decay and the gravitational binding energy

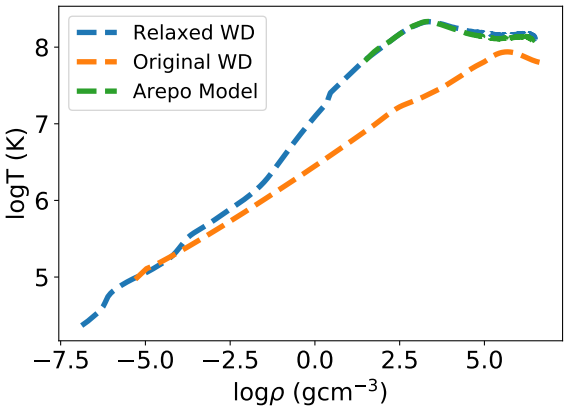

Figure 2. Comparison of temperature-density profiles for the Type-Ia remnant, the original white dwarf in MESA, and the Arepo profile which only extends till $\log(\rho) = 1$

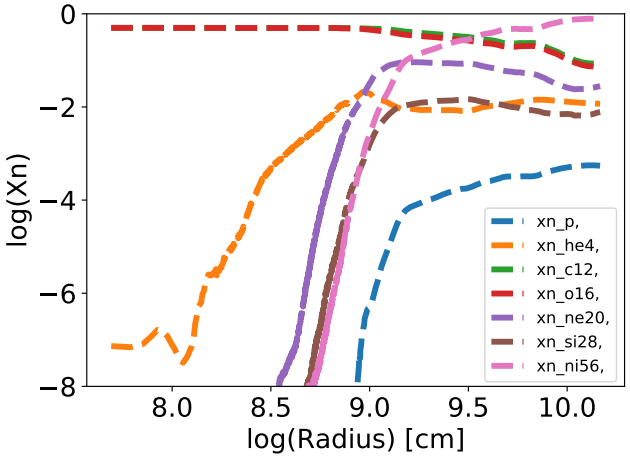

Figure 3. Main elements and their composition profiles as a function of radius

and entropy we needed to employ multiple subroutines of MESA, which we now discuss here.

3.1.1 Nuclear Reaction networks

We use multiple networks for this work. In the beginning used basic_net with added isotopes and reactions of Fe-56, O-16 and Ne-22. We used this as a probe against which future models with elemental burning could be compared. When considering burning our final models used the approx21_plus_co56 as our main network.

3.1.2 Opacities

The energy transport within a star is dependent on its opacity. The inverse of the opacity is defined as the sum of the inverses of the opacities due to conduction and radiation processes, and can be written as:

$$\frac{1}{\kappa} = \frac{1}{\kappa_{\rm cond}} + \frac{1}{\kappa_{\rm rad}} \tag{2}$$

The default MESA opacities are in form of tables for a given set of composition, temperature, and density known as OPAL tables (Iglesias & Rogers 1993a). These are known as Type-I opacities when metals are assumed to be present in scaled solar abundances. For C/O enriched compositions produced by He burning Type-II tables are available. In the beginning we operated with these opacities. However, as our WD surface is polluted due to the supernova ejecta, no precomputed opacity tables are available that accurately reflect the unusual surface composition of our models. To deal with this we add the calculation of monochromatic opacities to our MESA code which are taken from the Opacity Project (Seaton 2005). We go up to temperatures of $\log T \approx 7.5$, wherein the surface opacities can be recomputed during the evolution.

3.1.3 Helium mass fraction

During the course of this work it was found that the donor white dwarf has internal mixing of Helium due to shear forces caused by the material leaving the star when it fills its Roche lobe. This mixing can be seen in the composition profile of Helium in Fig. 3 and in Fig.4 which shows a snapshot of the AREPO simulation. This mixing is not yet well studied, and therefore, as a probe of this we not only use the normal Helium mass fractions we get from Arepo simulations but also include maximum limits of 5-10 times the Helium mass fraction (an upper limit of 0.03 solar masses of Helium).

3.2 Evolution with Iron

To have a baseline with which to compare our models, we assumed that all the Ni-56 had decayed to Fe-56, and used the composition profile of Ni-56 as the profile for Fe-56. This assumption is physically valid on the surface since Ni-56 has a half-life of 6.10 days, while Co-56 has a half-life of 77.7 days (Firestone et al. 1999), such that in the long term evolution all the Ni-56 is converted into Iron. In Fig. 5 and Fig. 6 we show the difference in the model evolution when running it without elemental burning (only mixing happens), and evolving it with burning but with different amounts of He-4. The 10 times He-4 mass fraction contributes around 0.03 solar masses of He-4. The main evolutionary difference is due to the Helium flash that significantly increases the stellar radius starting around a 1000 years. This is particularly long lasting in the case with 10 times the Helium amount, where this puffing up continues for around 10^5 years.

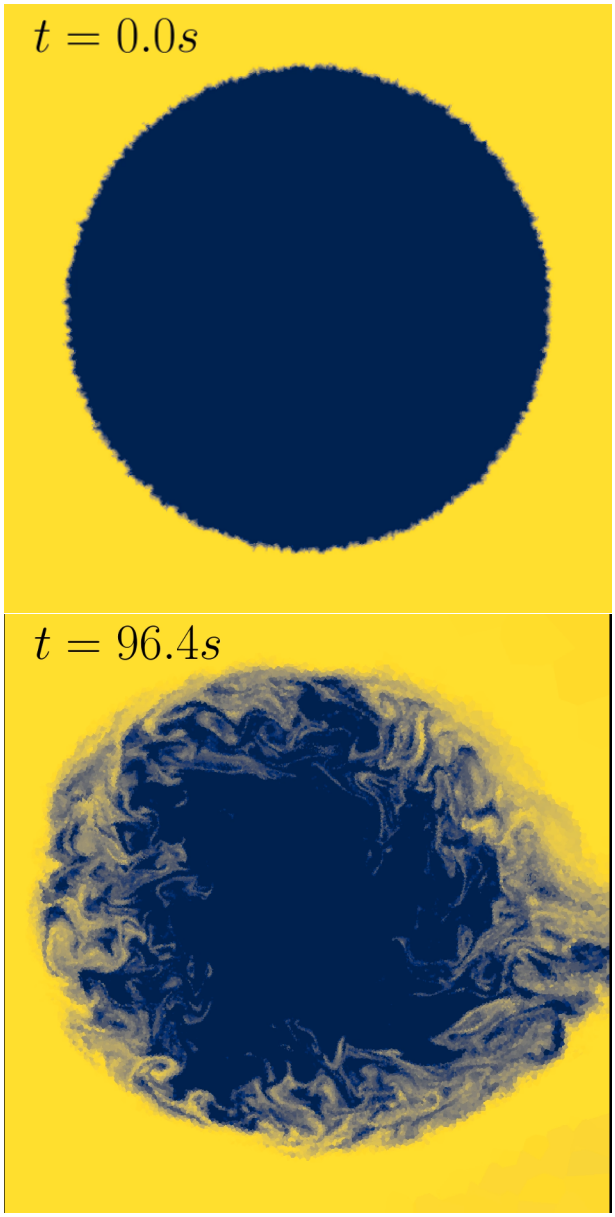

Figure 4. Top: Helium Mass fraction at the beginning of the simulation showing no mixing. Bottom: Mixing of Helium in the donor due to sheer forces caused by the accretion stream. The yellow represents the high Helium content with a mass fraction of 1 at the surface while the blue represents lower mass fraction of Helium close to 10^{-4} mass fraction. During the accretion the Helium from the surface seeps into the deeper layers of the donor.

3.3 Evolution with Ni-56

Once our Fe-56 models had evolved we started with Ni-56 in the atmosphere.

3.3.1 Using tabulated opacities

We turned on burning and decay, along with a super Eddington wind (wind factor of 0.9 and scaling factor of 1), which was required to allow for mass loss due to energy injection from the decay of Ni-56. As expected Ni-56 decays quickly and leads to a mass loss of roughly 0.01 $M_\odot$. This surface mass loss delays the Helium flash slightly because the layers containing He are less compressed due

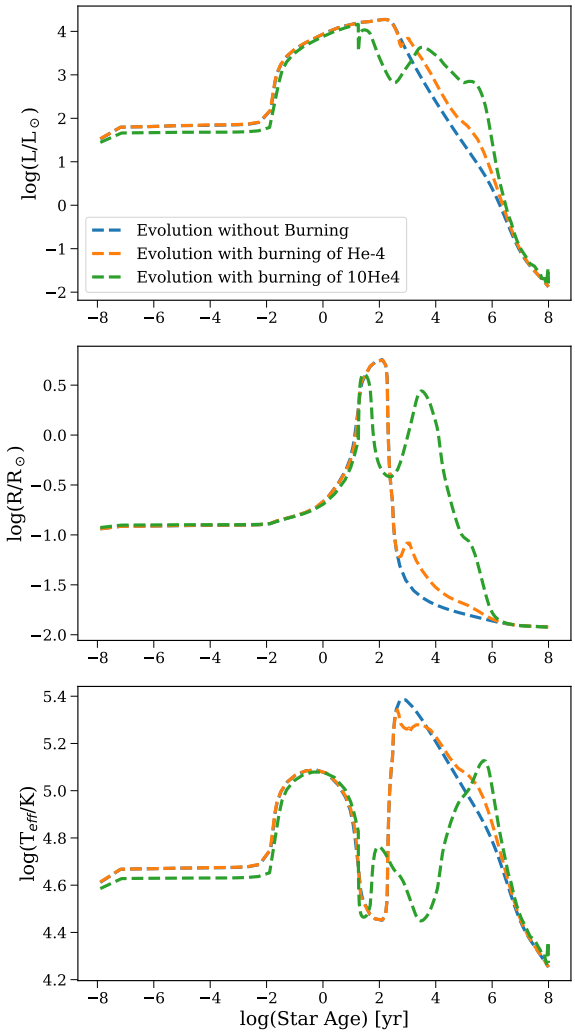

Figure 5. Evolutionary quantities of the model with Iron instead of Ni-56 as a function of its age

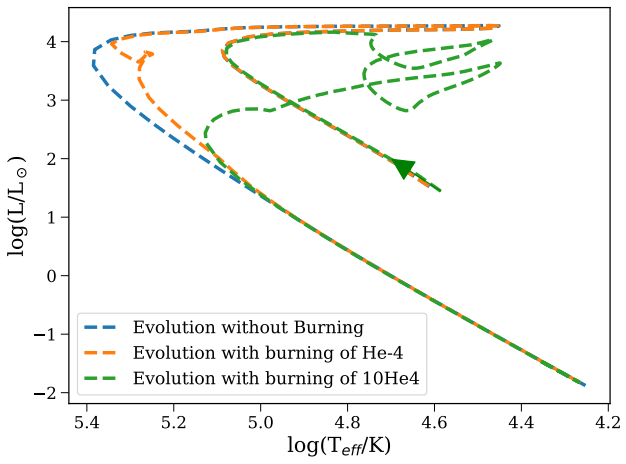

Figure 6. HR diagram of the model with Iron instead of Ni-56 showing a comparison without any burning and burning with different quantities of Helium. The arrow shows the starting track

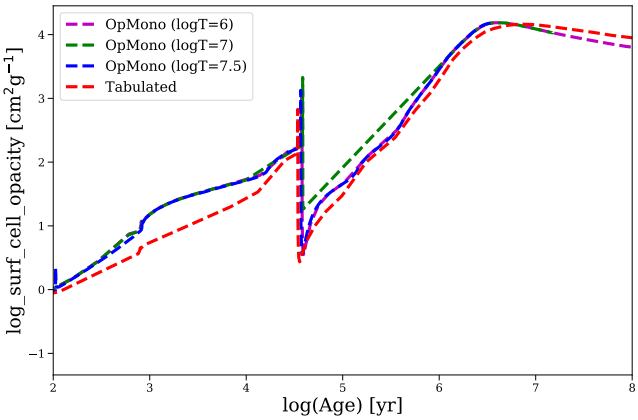

Figure 7. The surface opacity of the star as a function of its age for different limits of the Temperature up to which the opacities are calculated

to the lower mass of overlying material. The stellar radius increases less than it did for the Fe-56 case, but the increase happens for two orders of magnitude longer time. After the Helium has been burnt, the star reaches the white dwarf cooling track.

3.3.2 Using Op-mono

We then switch to the monochromatic opacity module to see the effect of calculating opacities more accurately on the fly, based on the density, temperature, and mass fraction profiles.

We run the same models again as we did with the tabulated opacities. Our initial settings included:

```
P_extra_factor = 1.2
high_logT_op_mono_full_on = 6.0
high_logT_op_mono_full_off = 6.4
```

The inlist controls of full_on and full_off define the temperature limits up to which the opacities are calculated using the op_mono package. Above these temperatures (deeper within the star) the opacities are tabulated Type II opacities. We tested different limits for temperatures at which OP mono opacities were applied, up to logT = 7.5. However, we find no significant difference between these different limits. While the surface luminosities and temperatures change slightly the difference is insignificant within the uncertainty one expects purely due to the models. The different surface opacities as a function of the stellar age are shown in Fig. 7. The slight difference is due to the difference in elemental mixing as a function of the opacities from the inside of the star.

In Fig. 8 and Fig. 9, we plot the evolution of the stars for different Helium content and different opacities along with the 4 new D-6 white dwarfs from El-Badry et al. (2023) and with an estimate for the 3 D-6 stars from Shen et al. (2018), assuming a temperature in the range of 7000-9000 K and a radius of the order 0.10-0.20 $R_\odot$. The latter is similar to what was found for D6-2 by Chandra et al. (2022). The luminosities are calculated in terms of solar luminosity using:

$$L/L_\odot = (R/R_\odot)^2 \frac{T_{\rm eff}}{5800\,{\rm K}} \tag{3}$$

The new D-6 stars of El-Badry et al. (2023) which are much hotter seem to lie within the parameter space of our evolutionary models, where the evolutionary age after leaving the supernova is

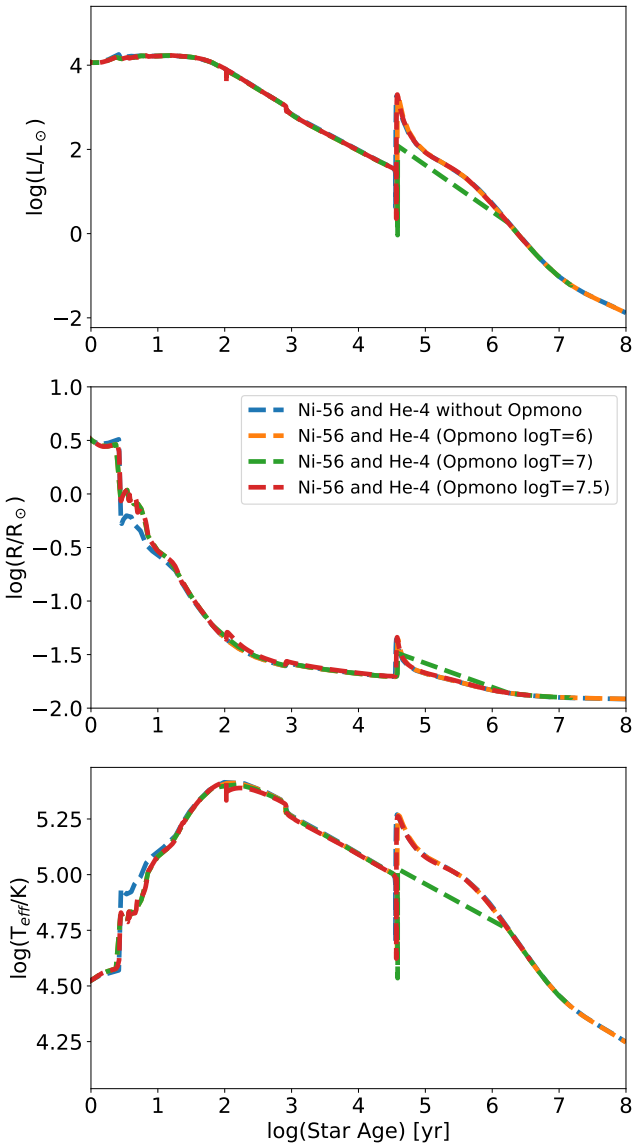

Figure 8. Evolutionary quantities of the model with Ni-56 as a function of its age

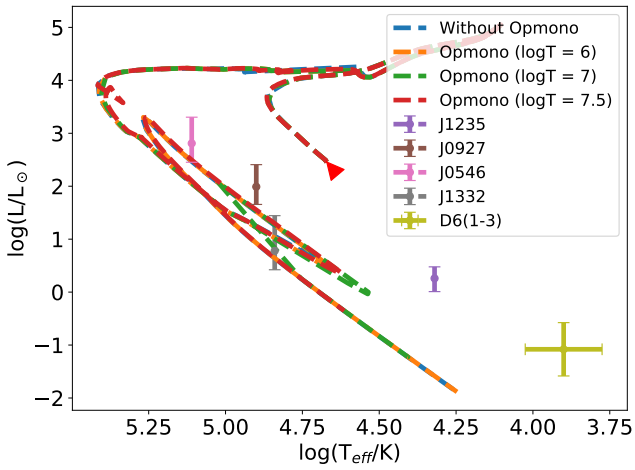

Figure 9. HR diagram of the model with Ni-56 showing a comparison with different quantities of Helium. The individual points also show the D6 observed stars from El-Badry et al. (2023) and Shen et al. (2018)

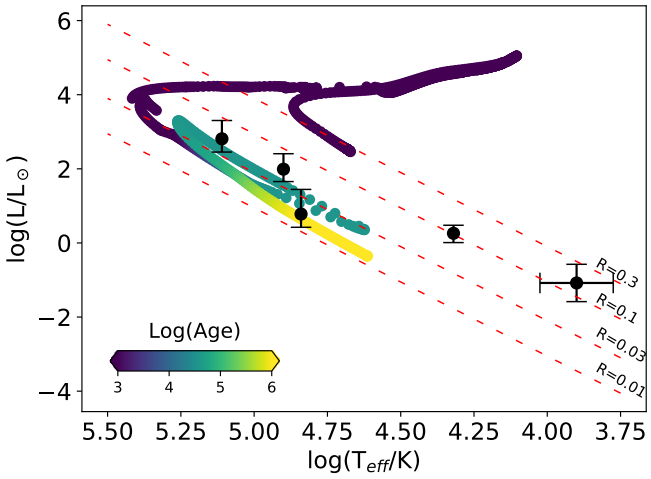

Figure 10. HR diagram of the model with Ni-56 with opacities calculated using op_mono until $\log T = 7.5K$. The individual points also show the D6 observed stars from El-Badry et al. (2023) and Shen et al. (2018)

predicted to be around $10^4 - 10^6$ yrs. The differences due to new opacity calculations are so small that they are barely visible in the plot and the two evolutionary tracks with and without monochromatic opacities are the same.

Our final HR diagram with monochromatic opacities up to $\log T = 7.5$K is shown in Fig. 10. The colorbar shows the ages from 10^3 to 10^6 years. As the stars travel at around 2000 kms^{-1}, they would be too far to observe after a few million years. We also plot the luminosity-temperature lines for constant radii using the black body law given by equation 3.

4 FUTURE WORK

One of the primary goals of this project was to model the evolution of a white dwarf polluted by supernova ejecta. For this purpose the composition and temperature-density profiles were directly taken from the Arepo simulations. However Arepo only simulates the stars once they are close enough to each other such that the Roche lobe of the donor can be filled. These stars are therefore provided with heating terms to get them to the right configuration. This makes the simulation neither easy to scale nor easy to apply to other problems, especially since one of the Arepo simulations takes almost a month to perform.

To allow for the possibility of scaling such a problem and making it more physically applicable, one can look at the relative difference between the composition/entropy of the donor white dwarf before and after the supernova. This entropy and composition difference comes entirely from the primary and is therefore scalable to other masses of donor white dwarfs as well as to other scenarios where the companion might not be a white dwarf but another compact object such as a subdwarf (whether such a configuration can exist is a question for the future as well). To this attempt we show in Fig. 11 the entropy profiles of the star before and after the supernova, a

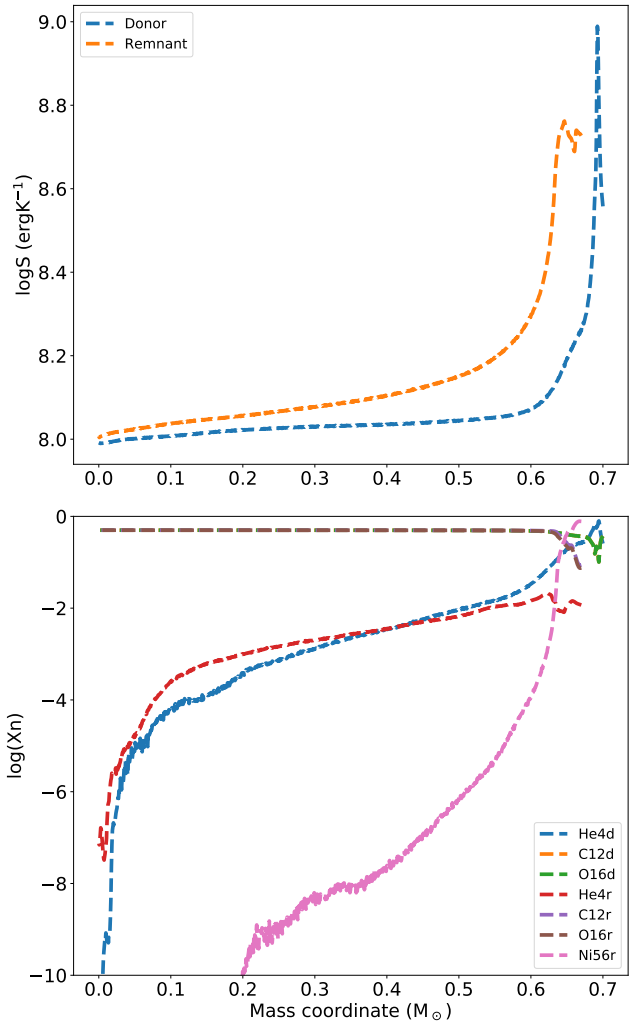

Figure 11. The entropy and composition profiles of the donor before and after the supernovas, referred to with the letter 'd' before and 'r' after. The bottom most panel shows the composition profiles after the Carbon and the Nickel mass fractions become equal near the surface

difference of which can be provided in MESA as a heating term over a physically valid assumption of time period.

5 CONCLUSIONS

In this report we have shown a proof of concept evolution of a runaway white dwarf created from a D-6 detonation scenario. We used composition and temperature-density profiles of the white dwarf from the hydrodynamical simulations made in Arepo. We were able to ingest these into MESA and relax a $0.67 M_\odot$white dwarf to these profiles. This relaxed white dwarf was then evolved to 100 Myrs. When compared with observations of such stars we were able to confirm 3 of the new found observations to lie close to our evolutionary tracks, whereas 4 of them (including D6-1 to D6-3) were not found to fit.

Since the composition of these stars is different we utilized the monochromatic opacities in MESA, which calculate opacities for different compositions during the run instead of using the Type-II opacities which are used by default in MESA. We found no significant difference in the calculations. This is probably because after some initial convective and thermohaline mixing, the overall mass composition is still primarily Carbon and Oxygen, in which case the new opacities become similar to the tabulated ones.

Finally we show how this problem may be rescaled by using the difference of entropy of the donor white dwarf such that multiple evolutionary models with different masses may be created.

ACKNOWLEDGEMENTS

We would like to thank the Kavli Summer program which took place in the Max Planck Institute for Astrophysics in Garching in July 2023. The primary author also thanks Dr. Selma de Mink for assigning this project to him.

Modules for Experiments in Stellar Astrophysics (MESA Paxton et al. 2011, 2013, 2015, 2018, 2019; Jermyn et al. 2023). The MESA EOS is a blend of the OPAL (Rogers & Nayfonov 2002), SCVH (Saumon et al. 1995), FreeEOS (Irwin 2004), HELM (Timmes & Swesty 2000), PC (Potekhin & Chabrier 2010), and Skye (Jermyn et al. 2021) EOSes.

Radiative opacities are primarily from OPAL (Iglesias & Rogers 1993b, 1996), with low-temperature data from Ferguson et al. (2005) and the high-temperature, Compton-scattering dominated regime by Poutanen (2017). Electron conduction opacities are from Cassisi et al. (2007) and Blouin et al. (2020).

Nuclear reaction rates are from JINA REACLIB (Cyburt et al. 2010), NACRE (Angulo et al. 1999) and additional tabulated weak reaction rates Fuller et al. (1985); Oda et al. (1994); Langanke & Martínez-Pinedo (2000). Screening is included via the prescription of Chugunov et al. (2007). Thermal neutrino loss rates are from Itoh et al. (1996).

REFERENCES

Angulo C., et al., 1999, Nuclear Phys. A, 656, 3
Bauer E. B., White C. J., Bildsten L., 2019, ApJ, 887, 68
Blouin S., Shaffer N. R., Saumon D., Starrett C. E., 2020, ApJ, 899, 46
Cassisi S., Potekhin A. Y., Pietrinferni A., Catelan M., Salaris M., 2007, ApJ, 661, 1094
Chandra V., et al., 2022, MNRAS, 512, 6122
Chugunov A. I., Dewitt H. E., Yakovlev D. G., 2007, Phys. Rev. D, 76, 025028
Cyburt R. H., et al., 2010, ApJS, 189, 240
El-Badry K., et al., 2023, arXiv e-prints, p. arXiv:2306.03914
Ferguson J. W., Alexander D. R., Allard F., Barman T., Bodnarik J. G., Hauschildt P. H., Heffner-Wong A., Tamanai A., 2005, ApJ, 623, 585
Firestone R. B., Ekstrom L. P., Chu S. Y. F., 1999, in APS Division of Nuclear Physics Meeting Abstracts. APS Meeting Abstracts. p. CE.13
Fuller G. M., Fowler W. A., Newman M. J., 1985, ApJ, 293, 1
Geier S., et al., 2015, Science, 347, 1126
Hirsch H. A., Heber U., O'Toole S. J., Bresolin F., 2005, A&A, 444, L61
Iglesias C. A., Rogers F. J., 1993a, ApJ, 412, 752
Iglesias C. A., Rogers F. J., 1993b, ApJ, 412, 752
Iglesias C. A., Rogers F. J., 1996, ApJ, 464, 943
Irwin A. W., 2004, The FreeEOS Code for Calculating the Equation of State for Stellar Interiors, `http://freeeos.sourceforge.net/`
Itoh N., Hayashi H., Nishikawa A., Kohyama Y., 1996, ApJS, 102, 411
Jermyn A. S., Schwab J., Bauer E., Timmes F. X., Potekhin A. Y., 2021, ApJ, 913, 72
Jermyn A. S., et al., 2023, ApJS, 265, 15
Kuchner M. J., Kirshner R. P., Pinto P. A., Leibundgut B., 1994, ApJ, 426, L89
Langanke K., Martínez-Pinedo G., 2000, Nuclear Physics A, 673, 481

Oda T., Hino M., Muto K., Takahara M., Sato K., 1994, Atomic Data and Nuclear Data Tables, 56, 231
Pakmor R., et al., 2022, MNRAS, 517, 5260
Paxton B., Bildsten L., Dotter A., Herwig F., Lesaffre P., Timmes F., 2011, ApJS, 192, 3
Paxton B., et al., 2013, ApJS, 208, 4
Paxton B., et al., 2015, ApJS, 220, 15
Paxton B., et al., 2018, ApJS, 234, 34
Paxton B., et al., 2019, ApJS, 243, 10
Potekhin A. Y., Chabrier G., 2010, Contributions to Plasma Physics, 50, 82
Poutanen J., 2017, ApJ, 835, 119
Raddi R., et al., 2019, MNRAS, 489, 1489
Rogers F. J., Nayfonov A., 2002, ApJ, 576, 1064
Saumon D., Chabrier G., van Horn H. M., 1995, ApJS, 99, 713
Seaton M. J., 2005, MNRAS, 362, L1
Shen K. J., et al., 2018, ApJ, 865, 15
Timmes F. X., Swesty F. D., 2000, ApJS, 126, 501
Weinberger R., Springel V., Pakmor R., 2020, ApJS, 248, 32
Zhang M., Fuller J., Schwab J., Foley R. J., 2019, ApJ, 872, 29

This paper has been typeset from a TEX/LATEX file prepared by the author.